ACS APPLIED MATERIALS & INTERFACES

Research Article

www.acsami.org

Molybdenum Nitride/N-Doped Carbon Nanospheres for Lithium-O_2 Battery Cathode Electrocatalyst

Kejun Zhang,[†,‡,§] Lixue Zhang,[†,§] Xiao Chen,[†] Xiang He,[#] Xiaogang Wang,[†] Shanmu Dong,[†] Lin Gu,[#] Zhihong Liu,[†] Changshui Huang,[†] and Guanglei Cui*[,†]

[†]Qingdao Institute of Bioenergy and Bioprocess Technology, Chinese Academy of Sciences, Qingdao 266101, China

[‡]University of Chinese Academy of Sciences, Beijing, 100039, China

[#]Beijing National Laboratory for Condensed Matter Physics, Institute of Physics, Chinese Academy of Sciences, Beijing 100080, China

Supporting Information

ABSTRACT: Molybdenum nitride/N-doped carbon nanospheres (MoN/N−C) are synthesized by hydrothermal method followed by ammonia annealing. The as-prepared MoN/N−C nanospheres manifest considerable electrocatalytic activity toward oxygen reduction reaction in nonaqueous electrolytes because of its nanostructure and the synergetic effect between MoN and N−C. Furthermore, the MoN/N−C nanospheres are explored as cathode catalyst for Li−O_2 batteries with tetra-(ethylene glycol) dimethyl ether as the electrolyte. The assembled batteries deliver alleviated overpotentials and improved battery lifespan, and their excellent performances should be attributed to the unique hierarchical structure and high fraction of surface active sites of cathode catalyst.

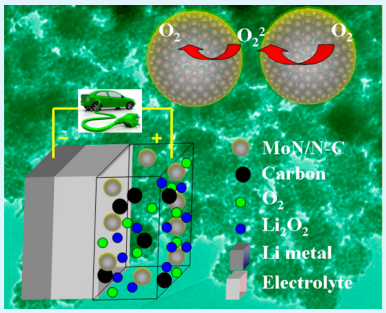

KEYWORDS: *MoN/N−C nanospheres, synergetic effect, electrocatalytic activity, oxygen reduction reaction, Li−O_2 batteries*

INTRODUCTION

The oxygen reduction reaction (ORR) is an important electrochemical reaction in a variety of electrochemical energy storage and conversion devices such as fuel cells and metal-air batteries.[1−7] Recently, ORR in nonaqueous electrolyte has received considerable attention in rechargeable Li−O_2 battery, which represents an emerging energy storage system for electric vehicle applications due to its high theoretical energy storage capacity.[8−13] An ideal electrocatalyst should facilitate a complete reversibility of oxygen reduction/evolution reactions (ORR/OER) for ($2Li + O_2 \longleftrightarrow Li_2O_2$) with little negative impact to the electrolyte. Recently, several non-noble metal materials such as carbon materials,[14,15] metal oxides,[16,17] perovskite,[18,19] and pyrochlore[20,21] have been widely explored as efficient catalysts or promoters for potential application in Li−O_2 battery, which enhances battery efficiency and improves battery lifespan by reducing or eliminating electrolyte decomposition. However, despite continuous efforts, the role of the catalyst in promoting ORR (discharge) or OER (charge) in Li−O_2 batteries still remains controversial.

Due to their unique characteristics, transition metal nitrides have been shown to have excellent catalytic activities in a variety of reactions.[22−25] It is known that the catalytic and electronic properties of transition metal nitrides are governed by their bulk and surface structure and stoichiometry.[26] Among numerous transition metallic nitrides, MoN, which exhibits high Pt-like electrocatalytic activities, electronic conductivity and chemical stability, has recently attracted extensive attention for potential applications in fuel cell and Li−O_2 battery.[27−29] Bulk MoN usually exhibits limited ORR activity probably because of their large particle size and low specific surface area.[27] Some efforts have been made to enhance the electrocatalytic activity of MoN.[27−29] For instance, carbon-supported MoN nanoparticles have been developed to maximize the electroactive surface area of catalyst and improve their catalytic activity.[27]

As well-known, highly efficient catalyst needs high surface areas or high active sites as well as fast mass transfer of the reactants and products to and from the catalytic sites. Therefore, it is of great significance to further explore the catalytic activity by rational design and facile synthesis of nanostructured catalysts materials. Herein, the molybdenum nitride/N-doped carbon nanospheres (MoN/N−C) with much active sites and mesopores were designed to improve the ORR catalytic activity of MoN material. The MoN nanospheres are prepared by reduction of MoO_2 nanospheres in ammonia atmosphere with cyanamide as the structure confinement agent. Because of the unique structure and composition, the MoN/N−C nanosphere catalyst displays excellent electrocatalytic activity in nonaqueous electrolytes. It is demonstrated that an enhanced performance of the rechargeable Li−O_2 battery is obtained when MoN/N−C nanospheres are used as the cathode catalyst. Such a transition metal nitride could alleviate

Received: January 17, 2013
Accepted: April 1, 2013
Published: April 1, 2013

   dx.doi.org/10.1021/am400209u | ACS Appl. Mater. Interfaces 2013, 5, 3677−3682

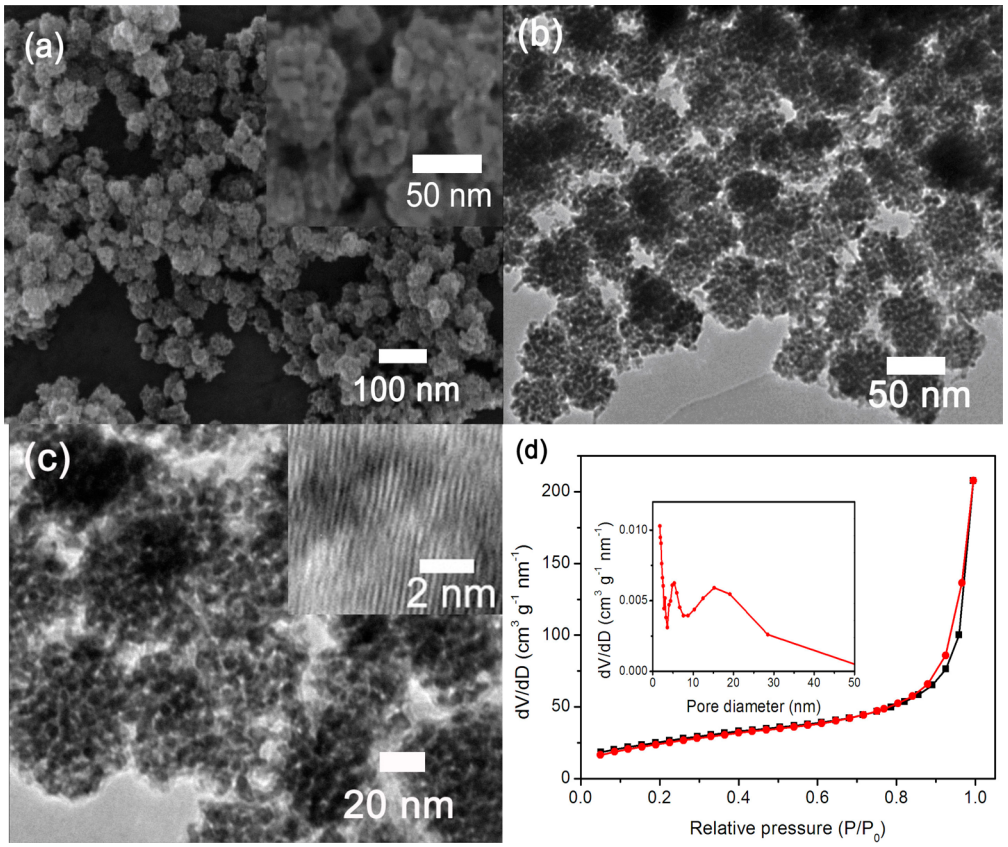

Figure 1. (a) Typical SEM image of MoN/N−C nanospheres. (b, c) Corresponding TEM image of MoN/N−C nanospheres, inset in c is HRTEM image of MoN/N−C nanospheres. (d) Nitrogen adsorption−desorption isotherms of MoN/N−C nanospheres and the pore-size distributions.

overpotentials during discharge and charge processes compared with super P, indicating a promising cathode catalyst candidate for nonaqueous Li−O_2 battery applications.

EXPERIMENTAL SECTION

Synthesis of MoN/N−C Nanospheres Catalyst. The MoN/N−C nanospheres were synthesized by a simple hydrothermal method combined with a heat teeatment at 700 °C under ammonia atmosphere. In a typical procedure, 50 mL of an aqueous solution containing 3.74 g of ammonium heptamolybdate tetrahydrate, 5 mL of ethylene glycol, and 5 g of polyvinylpyrrolidone (PVP, MW: 58 000) were mixed under continuous stirring for 1 h. The mixture solution was transferred into a 60 mL Teflon-lined autoclave and heated at 180 °C for 60 h. The precipitates were collected and washed with water and ethanol, and then dried at 60 °C. After that, 200 mg of the as-synthesized sample was mixed with 200 mg of cyanamide (NH_2CN, Aldrich) dissolved in 5 mL of absolute ethanol. The mixture was magnetically stirred for 2 h and dried at 80 °C to get a homogeneous bulk. Finally, the composite was annealed at 700 °C for 4 h in an ammonia flow to obtain the MoN/N−C nanospheres. As controls, free MoN and N-doped carbon (N−C) were prepared through the same procedure without adding PVP or Mo precursor in the first step.

Catalyst Characterization. X-ray diffraction (XRD) pattern was recorded in a Bruker-AXS Microdiffractometer (D8 ADVANCE) using Cu Kα radiation. The morphology of the MoN/N−C nanospheres was attained from field emission scanning electron microscopy (FESEM, HITACHI S-4800), and high-resolution transmission electron microscopy (TEM, JEOL 2010F). N_2 adsorption−desorption measurements were carried out at 77 K using a Quantachrome Autosorb gas-sorption system. X-ray photoelectron spectroscopy (XPS) was acquired using an ESCALab220i-XL spectrometer (VG Scientific) with Al Kα radiation in twin anode at 14 kV × 16 mA. Fourier transform infrared (FTIR) measurements were obtained on a JASCO FT/IR-6200 instrument from 2000 to 400 cm^{-1} with a resolution of 2 cm^{-1}.

Electrochemical Characterization. Li−O_2 cells consisted of a lithium metal anode and an O_2 electrode. The O_2 electrodes (typically 1.0 mg) were prepared by mixing 40 wt % catalysts with 40 wt % super P and 20 wt % polytetrafluoroethylene (PTFE) binders, or 70 wt % super P with 30 wt % PTFE. The samples were rolled into slices and cut into square pieces of 0.5 cm × 0.5 cm, and then pasted on a stainless steel current-collector under a pressure of 5 MPa. Electrochemical experiments were carried out by using a swagelok cell with a hole drilled only on the cathode of current collector to enable oxygen flow in. The Li−O_2 cells were assembled inside the glovebox under argon atmosphere (<1 ppm H_2O and O_2) by using a clean lithium metal disk (8 mm diameter) as anode, a glass-fiber and a polypropylene (Celgard 2400) as separators, 1 M LiTFSI in tetraethylene glycol dimethyl ether (TEGDME) as electrolyte. Galvanostatical discharge−charge experiments were tested on a LAND battery testing system. It is noted that the specific capacity was calculated based on the total mass of the oxygen electrode (electrocatalyst + super P + binder).

RESULTS AND DISCUSSION

The preparation of MoN/N−C nanospheres involves the hydrothermal synthesis of MoO_2 nanospheres, and the subsequent heat treatment under ammonia atmosphere. In the first step, MoO_2 nanospheres were synthesized by one pot hydrothermal treatment of a mixture containing ammonium heptamolybdate tetrahydrate, ethylene glycol, and PVP. The formation of MoO_2 is confirmed by XRD experiment (see Figure S1 in the Supporting Information). The SEM, TEM, and nitrogen adsorption−desorption experiments (as shown in Figures S2 and S3 in the Supporting Information) indicates that

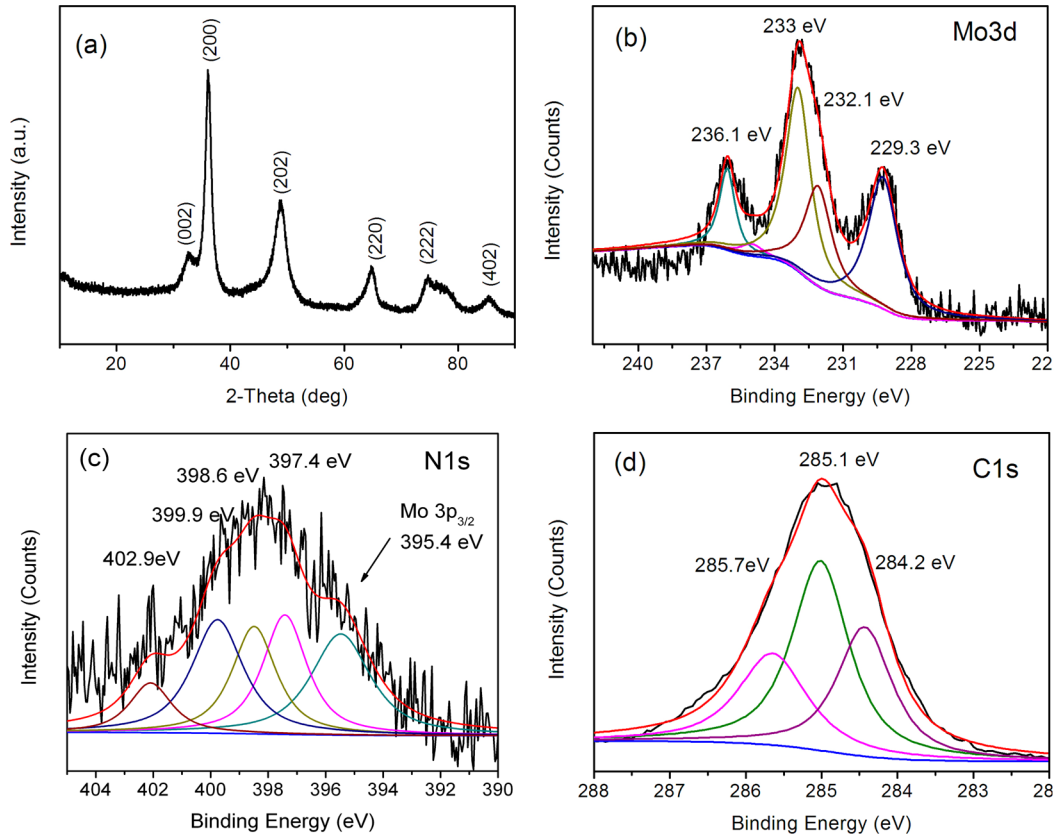

Figure 2. (a) XRD pattern of MoN/N−C nanospheres. (b) XPS spectra of Mo 3d, (c) N 1s, and (d) C 1s binding energy region of MoN/N−C nanospheres.

the as-prepared MoO_2 sample consists of nanospheres. It is inferred that primary MoO_2 nanocrystals with several nanometers are first formed in the solution by the reduction of ammonium heptamolybdate tetrahydrate with ethylene glycol; afterward, the MoO_2 nanospheres are generated by assembly of the primary nanocrystals to lower the system energy.[30−32] In this synthetic procedure, adequate PVP is introduced as capping agent to prevent the primary MoO_2 nanocrystals growing larger, as well as soft template to direct the assemble of MoO_2 nanospheres.

Then, as-prepared MoO_2 nanospheres were subsequently heated to 700 °C under ammonia atmosphere using cyanamide to retain the morphology,[33] the well-crystallized MoN/N−C nanospheres were obtained. The morphology of as-prepared MoN/N−C nanospheres was investigated by SEM and TEM. SEM image (Figure 1a) reveals that the samples consist entirely of uniform nanospheres with diameter of around 50 ± 5 nm. The high-magnification SEM image (Inset in Figure 1a) shows that these nanospheres are consisted of many primary nanocrystals, retaining the morphology of MoO_2 nanosphere. From the TEM results (Figure 1b, c), it can be clearly seen that the obtained MoN/N−C nanospheres with mesopores are formed by the assembly of many primary nanoparticles, and the primary building blocks of the MoN/N−C nanospheres has a size of 3−5 nm. The high-resolution TEM (HRTEM) image demonstrates the well-textured and single-crystalline nature of the primary MoN nanoparticles in MoN/N−C (Inset in Figure 1c). The porosity of the MoN/N−C nanospheres is determined by nitrogen sorption measurement (Figure 1d). The N_2 adsorption−desorption isotherms of materials is identified as Type IV isotherm, indicating characteristics of porous framework. The pore sizes of Barrett−Joyner−Halenda (BJH) are obtained from the isotherm range from 2 to 20 nm. In addition, BET analysis shows that MoN/N−C nanosphere sample possesses a specific surface area of 93 m^2 g^{-1}. The nanostructure of the MoN/N−C nanospheres endow them with more catalytic sites exposed to oxygen molecules and the great possibility of efficient mass transport, thus results in an enhancement of ORR activity.

The crystal structure of the MoN/N−C nanospheres was further examined with XRD. Figure 2a shows the power XRD pattern of the as-prepared MoN nanocrystals. The diffraction peaks could be indexed to the (002), (200), (202), (220), (222), and (402) plane reflections of MoN. All the diffraction peaks agree well with the standard diffraction data for the bulk MoN (JCPDS No. 77−1999). The oxidation states of elements in MoN/N−C sample were investigated by X-ray photoelectron spectroscopy (XPS). The XPS spectra confirm the existence of Mo, N, and C elements in the sample (Figure 2b-d). In addition, the energy dispersive X-ray (EDX) spectra shown in Figure S6 in the Supporting Information also indicate the presence of Mo, N, and C in the sample. It is worth noting that C in the sample should be derived from the carbonization of PVP and cyanamide during heat treatment. A Mo 3d peak at about 229.3 eV (Figure 2b) and a binding energy about 397.4 eV for the N 1s signal (Figure 2c) suggest the formation of Mo−N bond. As shown in Figure 2c, the deconvoluted bands of N 1s at around 398.6, 399.9, and 402.9 eV, represent pyridinic, pyrrolic and graphitic types of N, which confirmed the presence of doped N atoms in the carbon. A shoulder peak at 395.4 eV should be attributed to the binding energy of Mo $3p_{3/2}$. The C 1s core level can be resolved into three

dx.doi.org/10.1021/am400209u | ACS Appl. Mater. Interfaces 2013, 5, 3677−3682

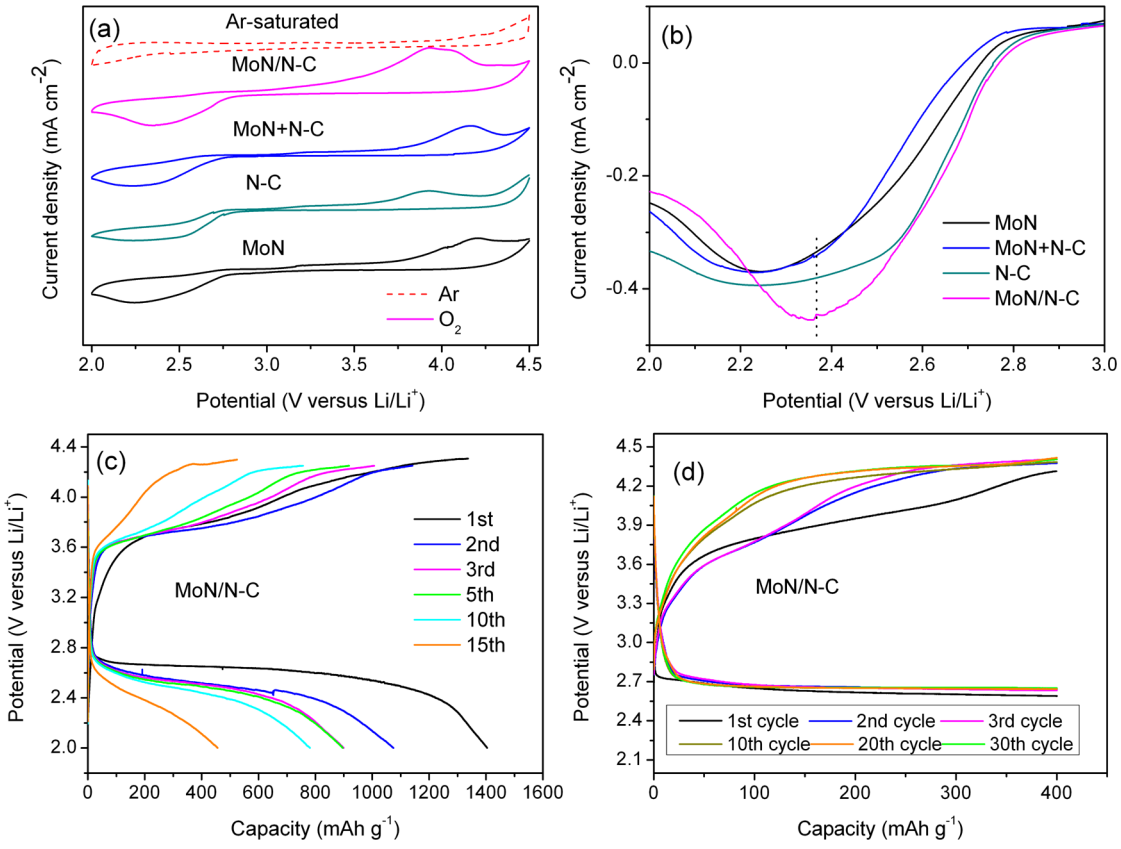

Figure 3. (a) CV curves of Li−O2 batteries with MoN/N−C, MoN, N−C, and MoN + N−C in TEGDME electrolyte containing 1 M LiTFSI at a scan rate of 0.2 mV s^{-1}. (b) ORR catalytic activity of the MoN/N−C, MoN, N−C, and MoN+N−C in 1 M LiTFSI/TEGDME. (c) Discharge and charge voltage profiles of the MoN/N−C-based cell at various cycles at a current density of 0.1 mA cm^{-2} in the voltage windows between 2.0 and 4.3 V. (d) Voltage profiles of 30 discharge−charge cycles at 400 mA h g^{-1} at the current density of 0.1 mA cm^{-2}.

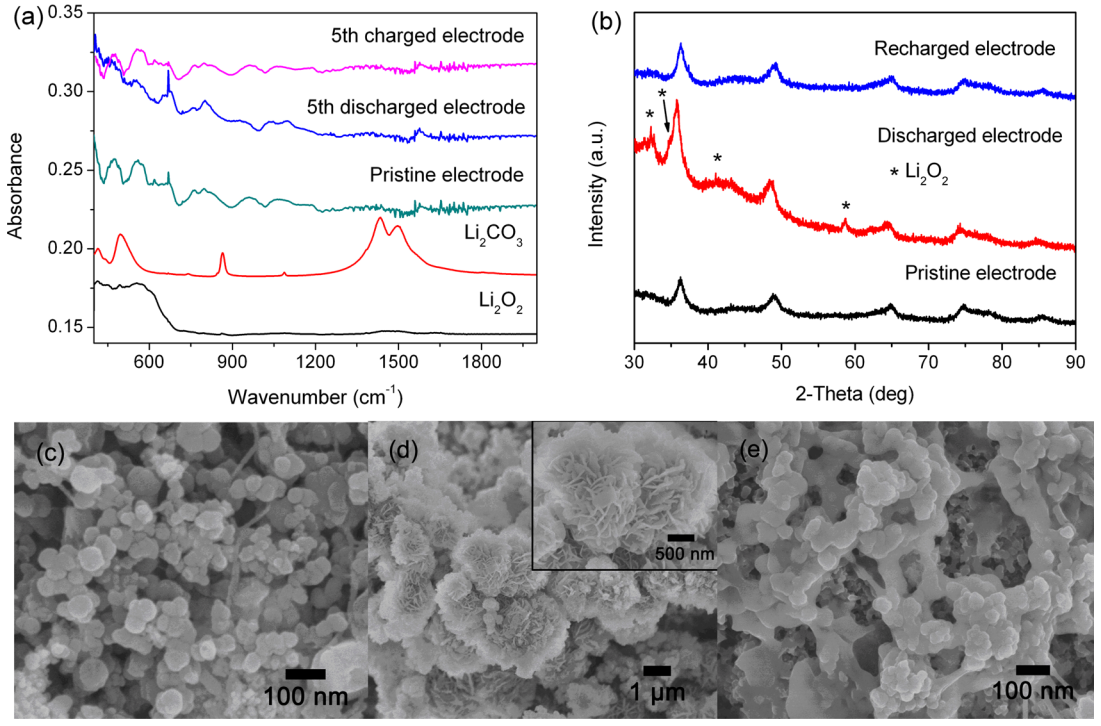

Figure 4. (a) FTIR spectra of MoN/N−C-based cathode at the 5th discharge and recharge. (b) XRD patterns for pristine, discharged, and subsequent charged cathodes in Li−O_2 batteries using an electrolyte containing 1 M LiTFSI in TEGDME. SEM images of (c) pristine electrode, (d) discharged electrode, and (e) the recharged electrode.

dx.doi.org/10.1021/am400209u | ACS Appl. Mater. Interfaces 2013, 5, 3677−3682

components centered ~284.2, 285.1, and 285.7 eV, representing that C is partially doped with N in sp^2–sp^2C, N–sp^2C and N–sp^3C type bonds, respectively.[34] These results confirm that the obtained samples are MoN/N–C nanospheres in our synthetic procedure.

To explore the ORR catalytic activity of the MoN/N–C nanospheres in nonaqueous electrolyte, we tested CV curves from 4.3 to 2 V in a configuration of nonaqueous Li–O_2 batteries (Figure 3a). Featureless CV curve is observed for MoN/N–C electrode in the Ar-saturated solution, whereas in the O_2-saturated solution, MoN/N–C electrode exhibits a high ORR onset potentials (~2.9 V) and obvious ORR/OER peaks. The MoN/N–C nanospheres exhibited higher ORR onset potentials and higher ORR peak current than those of the MoN, N–C and the physical mixture of MoN and N–C catalyst, implying that a synergetic effect between MoN and N-doped carbon in MoN/N–C nanospheres plays an important role in ORR catalytic activity. The electrochemical results suggested that MoN/N–C nanospheres could be an effective ORR catalyst for Li–O_2 batteries.

The efficiency of Li–O_2 batteries is greatly influenced by the ORR catalytic activity of cathode catalyst.[35] Inspired by the superior catalytic activity of MoN/N–C nanospheres, we tested the performance of a Li–O_2 battery with a MoN/N–C-based cathode (see Figure S7a in the Supporting Information). During discharge, the cell containing MoN/N–C catalyst demonstrated a relatively higher discharge voltage than that of super P, indicating an improvement in the catalytic activity of promoting lithium peroxide formation. In the following charge step, the effect of the MoN/N–C catalyst became more apparent, and the cell with MoN/N–C nanospheres showed a 0.55 V lower voltage than that of super P catalyst. The discharge and charge voltage profiles of the MoN/N–C-based electrode at various cycles at a current density of 0.1 mA cm^{-2} in the voltage windows between 2.0 and 4.3 V is presented in Figure 3c. The discharge capacity of the MoN/N–C-based Li–O_2 battery stabilizes above 790 mAh g^{-1} on the subsequent 10 cycles at a deep discharge to 2.0 V, it should be recalled that this is normalized to the total mass of the cathode (electrocatalyst + super P + binder). By contrast, the initial discharge capacity of Li–O_2 battery with pure super P cathode is 1150 mAh g^{-1}, and it dramatically drops to 280 mA h g^{-1} after the 10th cycling (see Figure S7b in the Supporting Information). As shown in Figure 3d, the cell showed good cycling ability over 30 cycles under a controlled capacity (400 mA h g^{-1}). These results hold great promise for creating porous MoN, which can clearly facilitate the OER and ORR processes by reducing the overpotentials at the Li–O_2 battery cathode.

The discharged and recharged electrodes after fifth cycle were also studied by FTIR spectroscopy (Figure 4a). Because there is obvious peak overlap between the pristine MoN electrode and Li_2O_2, it is hard to identify the existence of Li_2O_2 from the discharged electrode. There is no peak overlap between the pristine electrode and Li_2CO_3, therefore, the absence of Li_2CO_3 characteristic signals in the discharged electrode implies that the product was not Li_2CO_3. To further explore the insights of discharge and charge process of Li–O_2 battery with a MoN/N–C-based cathode, we analyzed the products after discharging and subsequent charging process using XRD and SEM (Figure 4b–e). According to the XRD patterns, Li_2O_2 crystalline phases were clearly observed in the discharged cathode. After fully recharging the cell to 4.3 V, the Li_2O_2 species were nearly eliminated. The reversibility of the Li_2O_2 formation/decomposition process was further confirmed by SEM analyses. The SEM image of the cathode surface before discharge shows many MoN/N–C nanospheres (Figure 4c). Then, it can be seen that the discharged products were deposited on the electrode, and the observed close-packed nanosheets are believed to be Li_2O_2 (circled regions in Figure 4d).[36] After charge, the Li_2O_2 nanosheets disappear and a relatively clean cathode is observed. However, some residual amorphous films still remain, which should be due to minor decomposition of electrolyte during charge (Figure 4e). Thus, Li_2O_2 is the dominant discharge product for Li–O_2 battery with a MoN/N–C-based cathode when the TEGDME-based electrolyte is used, and its formation/decomposition appears to be reversible. The remarkable ORR catalytic activity and high electronic conductivity of MoN/N–C should play an important role in improving the performance of Li–O_2 battery. In addition, such a catalyst with mesopores would produce more triple-phase (solid–liquid–gas phases) regions required for electrocatalysis, which effectively lower both electron and mass transport barriers and reduce the overpotential of discharge/charge process.

CONCLUSION

In summary, uniform N-doped carbon-coated MoN nanospheres with a size distribution of 50 ± 5 nm have been successfully synthesized by hydrothermal method followed by ammonia annealing. The MoN/N–C nanospheres consist of many tiny nanocrystals with a size of 3–5 nm. Because of the synergetic effects and the nanostructure, these MoN/N–C nanospheres deliver abundant surface active sites and excellent electrocatalytic activity in nonaqueous electrolytes. When evaluated as cathode materials for Li–O_2 battery, the MoN/N–C nanospheres exhibit excellent electrocatalytic performance for ORR/OER in Li–O_2 cells, including effectively lower the overpotentials and improve the battery lifespan. This may justify their promising application in Li–O_2 batteries. The novel synthesis method described here may be further extended to develop other metal nitrides for a wide of applications, such as energy storge, catalysis, and electrocatalysis.

ASSOCIATED CONTENT

Supporting Information

XRD pattern (Figure S1), SEM, TEM images (Figure S2), and BET (Figure S3) of MoO_2 nanospheres. XRD patterns of MoN nanoparticles and N–C (Figure S4). SEM images of MoN nanoparticles and N–C (Figure S5). EDX spectrum of the MoN/N–C nanospheres (Figure S6). Li–O_2 cell discharge/charge profiles of super P and MoN/N–C-based electrodes, and cycle performance of the super P-based cell (Figure S7). This material is available free of charge via the Internet at http://pubs.acs.org/.

AUTHOR INFORMATION

Corresponding Author

*E-mail: cuigl@qibebt.ac.cn.

Author Contributions

§Authors K.Z. and L.Z. contributed equally to this work.

Notes

The authors declare no competing financial interest.

■ ACKNOWLEDGMENTS

This work was supported by the key Research Program of the Chinese Academy of Sciences. Grant KGZD-EW-202-2, "100 Talents" program of Chinese Academy of Sciences, National Program on Key Basic Research Project of China (MOST2011CB935700), National Natural Science Foundation of China (21271180 and 21275151), and Doctoral Fund of Shandong Province (BS2012NJ011).

■ REFERENCES

(1) Steele, B. C. H.; Heinzel, A. *Nature* **2011**, *414*, 345−352.
(2) Lim, B.; Jiang, M.; Camargo, P. H. C.; Cho, E. C.; Tao, J.; Lu, X. M.; Zhu, Y. M.; Xia, Y. N. *Science* **2009**, *324*, 1302−1305.
(3) Su, D. S.; Sun, G. *Angew. Chem., Int. Ed.* **2011**, *50*, 11570−11572.
(4) Wu, G.; More, K. L.; Johnston, C. M.; Zelenay, P. *Science* **2011**, *332*, 443−447.
(5) Gong, K.; Du, F.; Xia, Z.; Durstock, M.; Dai, L. M. *Science* **2009**, *323*, 760−764.
(6) Lefevre, M.; Proietti, E.; Jaouen, F.; Dodelet, J. P. *Science* **2009**, *324*, 71−74.
(7) Suntivich, J.; Gasteiger, H. A.; Yabuuchi, N.; Nakanishi, H.; Goodenough, J. B.; Young, S. H.. *Nat. Chem.* **2011**, *3*, 546−550.
(8) Abraham, K. M.; Jiang, Z. A *J. Electrochem. Soc.* **1996**, *143*, 1−5.
(9) Girishkumar, G.; McCloskey, B.; Luntz, A. C.; Swanson, S.; Wilcke, W. *J. Phys. Chem. Lett.* **2010**, *1*, 2193−2203.
(10) Peng, Z. Q.; Freunberger, S. A.; Chen, Y. H.; Bruce, P. G. *Science* **2012**, *337*, 563−566.
(11) Shao, Y. Y.; Park, S.; Xiao, J.; Zhang, J. G.; Wang, Y.; Liu, J. *ACS Catal.* **2012**, *2*, 844−857.
(12) Wang, H.; Yang, Y.; Liang, Y.; Zheng, G.; Li, Y.; Cui, Y.; Dai, H. *Energy Environ. Sci.* **2012**, *5*, 7931−7935.
(13) Wu, G.; Mack, N. H.; Gao, W.; Ma, S. G.; Zhong, R. Q.; Han, J. T.; Baldwin, J. K.; Zelenay, P. *ACS Nano* **2012**, *6*, 9764−9776.
(14) Jung, H. G.; Hassoun, J.; Park, J. B.; Sun, Y. K.; Scrosati, B. *Nat. Chem.* **2012**, *4*, 579−585.
(15) Thotiyl, M. M. O.; Freunberger, S. A.; Peng, Z. Q.; Bruce, P. G. *J. Am. Chem. Soc.* **2013**, *135*, 494−500.
(16) Débart, A.; Paterson, A. J.; Bao, J.; Bruce, P. G. *Angew. Chem., Int. Ed.* **2008**, *47*, 4521−4524.
(17) Black, R.; Lee, J. H.; Adams, B.; Mims, C. A.; Nazar, L. F. *Angew. Chem., Int. Ed.* **2013**, *52*, 392−396.
(18) Zhao, Y. L.; Xu, L.; Mai, L. Q.; Han, C. H.; An, Q. Y.; Xu, X.; Liu, X.; Zhang, Q. J. *Proc. Natl. Acad. Sci. U.S.A.* **2012**, *109*, 19569−19574.
(19) Donner, W.; Chen, C.; Liu, M.; Jacobson, A. J.; Lee, Y. L.; Gadre, M.; Morgan, D. *Chem. Mater.* **2011**, *23*, 984−988.
(20) Oh, S. Y.; Black, R.; Pomerantseva, E.; Lee, J. H.; Nazar, L. F. *Nat. Chem.* **2012**, *4*, 1004−1010.
(21) Oh, S. H.; Nazar, L. F. *Adv. Energy Mater.* **2012**, *2*, 903−910.
(22) Shui, J. L.; Karan, N. K.; Balasubramanian, M.; Li, S. Y.; Liu, D. J. *J. Am. Chem. Soc.* **2012**, *134*, 16654−16661.
(23) Wu, H. B.; Chen, W. *J. Am. Chem. Soc.* **2011**, *133*, 15236−15239.
(24) Li, F. J.; Ohnishi, R.; Yamada, Y.; Kubota, J.; Domen, K.; Yamada, A.; Zhou, H. S. *Chem. Commun.* **2013**, *49*, 1175−1177.
(25) Dong, S. M.; Chen, X.; Gu, L.; Zhang, L. X.; Zhou, X. H.; Cui, G. L; Chen, L. Q. *ChemSusChem.* **2012**, *5*, 1712−1715.
(26) Chen, W. F.; Sasaki, K.; Ma, C.; Frenkel, A. I.; Marinkovic, N.; Muckerman, J. T.; Adzic, R. R. *Angew. Chem., Int. Ed.* **2012**, *51*, 6131−6135.
(27) Qi, J.; Jing, L. H.; Jiang, Q.; Wang, S. L.; Sun, G. Q. *J. Phys. Chem. C.* **2010**, *114*, 18159−18166.
(28) Li, G. R.; Song, J.; Pan, G. L.; Gao, X. P. *Energy Environ. Sci.* **2011**, *4*, 1680−1683.
(29) Dong, S. M.; Chen, X.; Zhang, K. J.; Gu, L.; Zhang, L. X.; Zhou, X. H.; Cui, G. L; Chen, L. Q. *Chem. Commun.* **2011**, *479*, 11291−11293.
(30) Teo, J. J.; Chang, Y.; Zeng, H. C. *Langmuir* **2006**, *22*, 7369−7377.
(31) Liu, B.; Zeng, H. C. *Small* **2005**, *1*, 566−571.
(32) Wang, Z. Y.; Chen, J. S.; Ting, Z.; Madhavi, S.; Lou, W. X. *Chem. Commun.* **2010**, *46*, 6906−6908.
(33) Dong, S. M.; Chen, X.; Gu, L.; Zhou, X. H.; Xu, H. X.; Cui, G. L.; Chen, L. Q. *ACS. Appl. Mater. Interfaces* **2010**, *3*, 93−98.
(34) Wang, H. B.; Zhang, C. J.; Liu, Z. H.; Wang, L.; Han, P. H.; Cui, G. L. *J. Mater. Chem.* **2011**, *21*, 5430−5434.
(35) Wang, L.; Zhao, X.; Lu, Y. H.; Xu, M. W.; Zhang, D. W.; Ruoff, R. S.; Stevenson, K. J.; Goodenough, J. B. *J. Electrochem. Soc.* **2011**, *158*, A1379−A1382.
(36) Li, Y. L.; Wang, J. j.; Li, X. F.; Geng, D. S.; Banis, M. N.; Tang, Y. J.; Wang, D. N.; Sun, X. L. *J. Mater. Chem.* **2012**, *22*, 20170−20174.